1-1-2012

Optical Coherence Tomography Detection of Shear Wave

Marjan Razani
Ryerson University

OPTICAL COHERENCE TOMOGRAPHY DETECTION OF SHEAR WAVE PROPAGATION

By

Marjan Razani

M.Sc. Iran University, 2001

Tehran, Iran

A thesis

presented to Ryerson University

in partial fulfillment of the

requirements for the degree of

Master of Science

in the Program of

Biomedical Physics

Toronto, Ontario, Canada, 2012

Author's Declaration

I hereby declare that I am the sole author of this thesis. This is a true copy of the thesis, including any required final revisions, as accepted by my examiners.

I authorize Ryerson University to lend this thesis to other institutions or individuals for the purpose of scholarly research.

I further authorize Ryerson University to reproduce this thesis by photocopying or by other means, in total or in part, at the request of other institutions or individuals for the purpose of scholarly research.

I understand that my thesis may be made electronically available to the public.

Marjan Razani

Abstract

Marjan Razani. “Optical Coherence Tomography detection of shear wave propagation”, M.Sc. Biomedical Physics, Ryerson University, Toronto, 2012

In this work, we explored the potential of measuring shear wave propagation using Optical Coherence Elastography (OCE). Shear waves were generated using a 20 MHz piezoelectric transducer transmitting sine-wave bursts of 400 μs, synchronized with the OCT swept source wavelength sweep. The acoustic radiation force was applied to two gelatin phantoms (differing in gelatin concentration by weight, 8% vs 14%, respectively). Differential OCT phase maps, measured with and without the acoustic radiation force, demonstrate microscopic displacement generated by shear wave propagation in these phantoms of different stiffness. The shear wave speeds for the 14% and 8% gelatin-titanium dioxide phantoms were 2.24 ± 0.06 m/s and 1.49 ± 0.05 m/s and also the shear modulus estimated using SW-OCE was 5.3±0.2 kPa and 2.3±0.1 kPa for the 14% and 8% gelatin-titanium dioxide phantoms, respectively. The results demonstrate the feasibility of this technique for measuring the mechanical properties of tissue.

Acknowledgements

I would like to sincerely thank my supervisor Dr. Michael Kolios for his support and confidence during this research. His excitement and enthusiasm about physics is not only motivating, but also highly contagious. I feel privileged to have worked with such a knowledgeable professional. I would also like to thank my supervisory committee, Dr. Victor X.D. Yang, Dr. Yuan Xu for their guidance during this research.

I would like to thank Dr. Adrian Mariampillai, Dr. Cuiru Sun ,Dr. Mathias Fink, Dr. Hassan Firoozmand, and Arthur Worthington for their contributions and discussions.

I would like to thank my mom and dad, for their support and for always encouraging me to pursue my dreams.

Table of Contents

List of Tables

List of Figures

List of symbols

C_p Longitudinal wave speed

ρ Density

K bulk modulus

μ Shear modulus

C_s Shear wave speed

F The acoustic radiation force

C The speed of sound in the medium

α The absorption coefficient of the medium

I The temporal average intensity at a given spatial location

L_c Coherence length

Δx lateral resolution

μ_2 Shear viscosity

ω Shear wave angular frequency

ν Poisson's ratio

E Young's modulus

$\Delta\varphi$ The phase shift between the two tracking location

Δr The distance between the two tracking locations

C_{group} Group Velocity

k The angular wavenumber

C_{phase} Phase Velocity

Chapter 1 Introduction

This chapter provides an introduction to the background of the thesis, including the principle of shear wave propagation in tissue and Optical Coherence Tomography (OCT).There has been great interest in measuring the shear modulus of tissues due to the large range of values of the parameter for soft tissues[1]. In this work, the proposed the imaging modality to detect shear wave propagation is OCT. Other methods that have been used to detect shear wave propagation include magnetic resonance imaging (MRI) and ultrasound.

1.1 Longitudinal and shear waves

A wave usually transfers energy from one point to other points [3]. Two types of mechanical waves of interest to this work are:

Longitudinal sound waves: For longitudinal sound waves, the particle motion is parallel to direction of propagation of the bulk wave. Such compressional waves propagate at a speed given by the equation:

$$C_{p=}\sqrt{\frac{\lambda+2\mu}{\rho}} \cong \sqrt{\frac{\lambda}{\rho}} \ (\approx 1500\,\frac{m}{s}) \qquad (1.1)$$

Where $\lambda = K + {}^{4}/_{3}\,\mu$

For most biological tissues the speed is ~1500 m/s.

Shear sound wave: For shear sound waves, the particle motion is perpendicular to direction of propagation of the bulk wave. Shear waves propagate at a speed given by the equation:

$$C_s = \sqrt{\frac{\mu}{\rho}} \quad , \tag{1.2}$$

where μ is shear modulus and ρ is density of medium.

Therefore for most biological tissues the shear wave speed is ($\approx 1 - 10\ \mathrm{m/s}$)

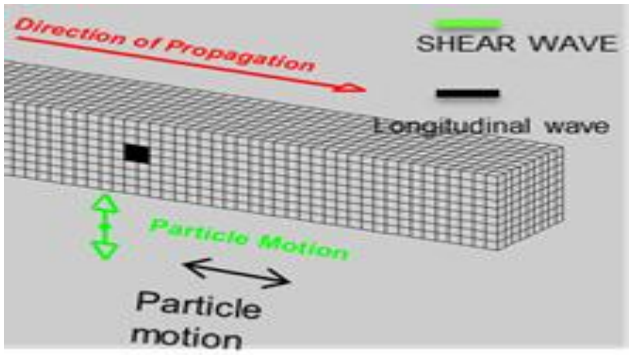

Figure 1-1-1: Longitudinal and shear waves. The black arrow shows the particle motion which is parallel with direction of propagation (longitudinal wave). The green arrow shows the particle motion which is perpendicular to direction of propagation (shear wave) adapted from [2].

When discussing the wave propagation velocity, there are two types of velocity on interest:

Group velocity: The group velocity is the velocity with which the overall shape of the wave's amplitudes can propagate. The propagation speed can be obtained by the envelope of the wave [3].

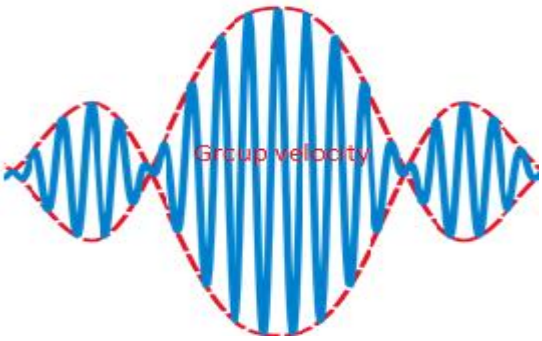

Figure 1-1-2: The propagation velocity of the signal envelope represents the group velocity adapted from [3]

The group velocity can be obtained by following equation:

$$C_{group}=\frac{\delta\omega}{\delta k} \quad , \tag{1.3}$$

where ω is the wave's angular frequency (usually expressed in radians per second), and k is the angular wavenumber (usually expressed in radians per meter) [3].

Phase velocity: The phase velocity is the velocity at which a frequency component travels.

The phase velocity also can be found by following equation, where ω is the wave's angular frequency and k is the angular wavenumber [4].

$$C_{phase}=\frac{\omega}{k}, \tag{1.4}$$

Shear waves cannot propagate in liquids. However, because most biological tissues have an elastic component, they can support shear waves. Shear waves can be produced by inducing a

sinusoidal excitation that displaces bulk tissue along the direction of the excitation. To recover the tissue shear modulus, two general categories of reconstruction methods have be used: 1. forward methods that minimize the difference between displacements calculated theoretically using models with assumed material properties and the displacements measured experimentally with an imaging device and 2. direct inversion of the differential equation of motion. These methods include the inversion of the Helmholtz Equation, which characterizes the shear wave propagation [5, 9], using algorithms that measure lateral time for peak-to-peak displacements [6], tracking the displacement field jitters that are associated with shear waves [7, 8], and using a variety of correlation-based algorithms [10, 11]. The speed of shear waves that propagate in soft tissues is directly related to the shear modulus of the material (Equation 4) [12, 13]. Traditional compression wave imaging methodologies, such as US, provide measurements based on the tissue bulk modulus, which is confined to a relatively small range for soft tissues. The shear modulus for soft biological tissues actually span a much larger range compared to the bulk modulus by several orders of magnitude [9, 14]. The use of the shear modulus as a cancer biomarker has been recently demonstrated using ultrasonic techniques [15]. The acoustic radiation force (ARF) of ultrasound propagating waves has been used to generate such mechanical excitations noninvasively.

1.2 Acoustic Radiation Force Impulse (ARFI)

The Acoustic Radiation Force (ARF) is produced by a change in the energy density of the incident acoustic field [6, 7]. The acoustic radiation force is generated by the transfer of momentum from the acoustic wave to the tissue. This can be achieved by using focused

ultrasound. The force is applied in the direction of the longitudinal wave propagation and the magnitude of the force can be approximated by:

$$F = \frac{2\alpha I}{C} \tag{1.5}$$

where F, kg/(s ^{2} cm ^{2}), is the acoustic radiation force, C (m/s) is the speed of sound in the medium, α (Np/m) is the absorption coefficient of the medium and I (W/cm^2) is the temporal average intensity at a given spatial location [8]. Figure 1 shows the principle of shear wave generation. Shear waves can be generated by using a focused impulse generated by an ultrasound transducer. The impulse creates a displacement in the direction of ultrasonic beam propagation which is largest at the transducer focus. After the impulse the material relaxes back to its original state producing a shear wave. The shear wave propagates in the direction perpendicular to the direction of the focused ultrasound propagation.

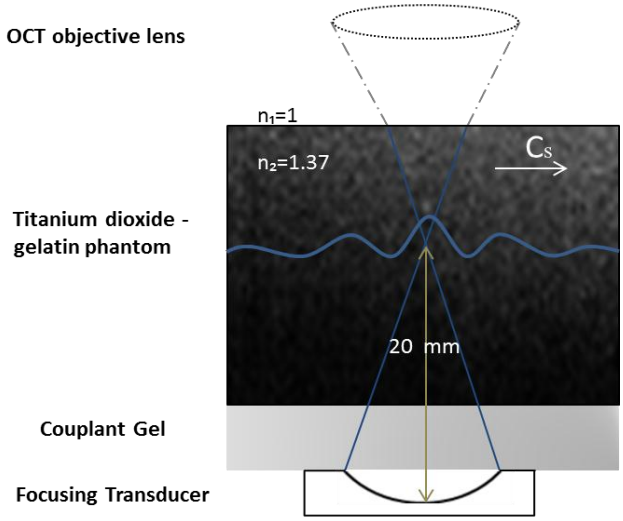

Figure 1-2: The principle of the generation of shear wave propagation using a focused ultrasound transducer. The OCT objective lens is related to the imaging device used in experiments to detect the shear wave propagation.

1.2.1 The nature of the shear wave produced with ARF

When the acoustic radiation force is applied to a given spatial volume for a short time duration, shear waves are generated that propagate away from the initial region of excitation (i.e. the focal spot region) [9]. Shear-wave propagation speed and attenuation are directly related to the mechanical properties of the tissue. Typical values for the speed of shear wave are of the order of a 1-10 m/s, and the attenuation coefficient of soft tissues are two or three orders of magnitude higher than that of compressional waves. Due to the high attenuation of shear waves, it is possible to generate the shear wave within a very limited area of tissue [9]. The spatial frequency content of the shear wave will be determined primarily be the width of the ultrasound beam (and not the time duration of the excitation unless the excitation duration approaches the natural time constants of soft tissues). This is turn dictates the frequency of the shear wave produced; smaller ARF beams produce higher frequency shear waves. In this thesis the transducer used to produce the ARF had a beam diameter of 245 μm (the depth of field was 2.94mm and a 20MHz sine-wave burst of 400μs was applied).

1.3 Imaging modalities used to detect shear wave propagation

There are several imaging modalities that have been used to detect shear wave propagation in tissue:1) ultrasound (and a variant of ultrasound imaging called supersonic shear wave imaging) 2) MRI and 3) Optical Coherence Tomography.

1.3.1 Ultrasound

Ultrasound can be used to measure bulk tissue displacement using algorithms that detect tissue motion. Shear waves can be created in a medium by using a focused transducer (such as an ultrasonic phased array or a single focused transducer) and then the tissue motion can be detected by using either the same transducer or other independent ultrasound pulse-echo imaging transducers [7]. Shear waves generated in this matter typically have low frequencies. Moreover, the speed of shear waves is smaller than the speed of the typical ultrasound longitudinal waves used in biomedical applications (equations 1.1 and 1.2).

To track the displacements generated by the excitation source (e.g. the ARF), a reference ultrasound A-line pulse is initially fired for tracking, followed by a high-intensity pulse used to generate the ARF, followed by a series of ultrasound A-line tracking pulses to monitor the resulting tissue displacement. To estimate the tissue displacements toward and away from the transducer, the normalized cross-correlation of the tracked echoes through time is used. Fig1.3 illustrates the schematics of SWEI (shear wave elasticity imaging) using ultrasound.

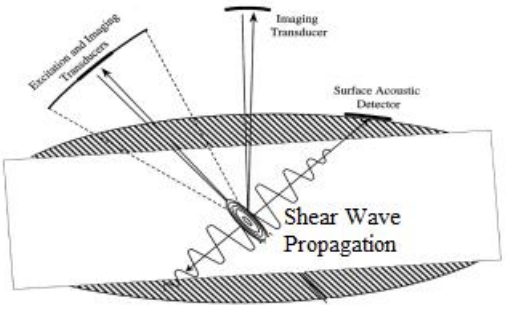

Figure 1-3: Schematic presentation of shear wave elasticity imaging (adapted from [9]). Ultrasound can be used to both generate shear waves in tissue, and to image the propagation of these waves.

1.3.2 Supersonic shear wave imaging

Large tissue displacements are required to generate shear waves of sufficient amplitude to be detected with the various imaging modalities. Therefore, high intensities are required for the acoustic radiation force pulses. One method to overcome this uses a shear source moving through the medium at a supersonic speed (greater than speed of the shear wave in tissue). This can be achieved by successively focusing the ultrasonic "pushing" ARF beam at different depths at a speed that is greater than the tissue shear wave speed. The result of the beam traveling faster than the shear wave is that all the resulting shear waves interfere constructively along a Mach cone creating planes of intense shear waves propagating in opposite directions, analogous to a "sonic boom" created by a supersonic aircraft. Figure 1.4 shows the principle of supersonic shear imaging. Supersonic shear wave imaging can provide the quantitative shear modulus mapping of an entire organ in less than 30 ms [16].

Pushing beam Imaging shear wave

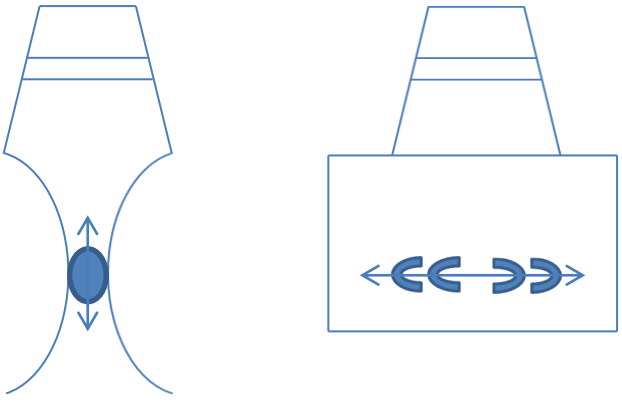

A B

Figure 1-4: A) An ultrasonic probe creates a force that displaces the tissue at the focal point. B) After relaxation of the displaced (pushed) tissue, a low frequency shear wave is generated and the tissue displacement is measured by tracking successive A-lines.

.

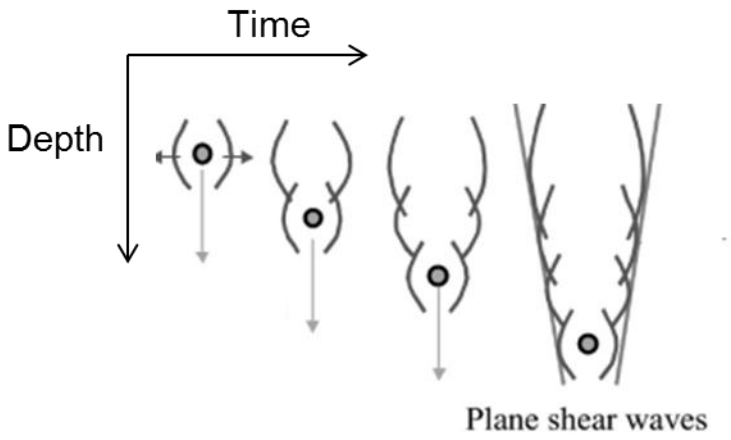

Figure 1-5: Generation of plane shear waves using the motion of a supersonic shear source. (Adapted from [16])

1.3.3 Magnetic resonance elastography (MRE)

Magnetic resonance elastography (MRE) is a recently developed technique that can detect small tissue displacements. The method combines a mechanically applied stress (using an actuator or the acoustic radiation force of an ultrasound pulse) with Magnetic Resonance Imaging (MRI) to measure displacement within the tissue or object. Magnetic resonance elastography usually combines MRI with mechanical waves to create a visual map, or

elastogram, which can measure the stiffness of body [17,18]. Moreover this is a non-invasive imaging modality that allows for the determination of the shear modulus (elastic modulus, shear stiffness) tissues *in vivo.*

This technique generate shear waves (with frequencies in the acoustic range), a phase-sensitive MR imaging sequence to detect the propagating waves and an algorithm to generate an elastic modulus map of the tissue of interest. In MRE, a phase-contrast MRI technique is used to spatially map and measure displacement patterns corresponding to harmonic shear waves with amplitudes of microns or less.

These quantitative techniques usually require long scan times, the acquisition of large amounts of data and sophisticated reconstruction algorithms including phase unwrapping and stiffness inversions to produce measurements of material properties. The time required to acquire and analyze the data depend on the amount of data and the type of algorithm[19].

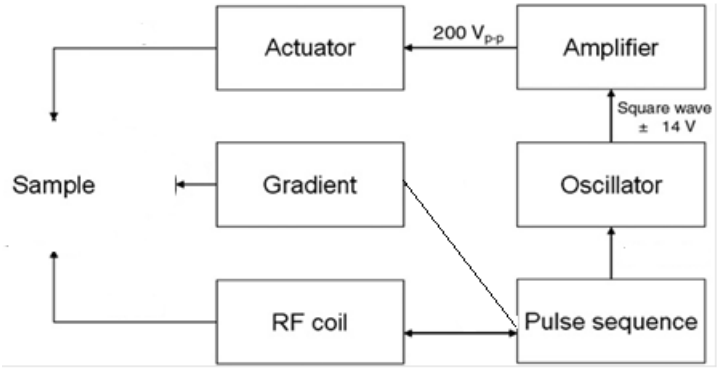

Figure 1-6: The schematics of MRE system. The pulse sequence controls MR such as Gradient and RF coil and shear-wave excitation. The pulse sequence also connect to the oscillator, which, in turn, feeds the amplifier with a square wave that activates the

mechanical actuator. The mechanical actuator movement is in synchrony with the bipolar gradient pulses used to acquire MR images (adapted from [20]).

1.3.4 Optical Coherence Tomography

Optical Coherence Tomography (OCT) provides imaging with histological resolution, which allows for the identification of micron sized morphological tissue structures. Optical coherence elastography (OCE) measures tissue displacement using OCT and benefits from the high resolution of OCT to generate high-resolution stiffness maps. In this work, we explore the potential of measuring shear wave propagation using OCT as an imaging modality to detect the shear wave propagation.

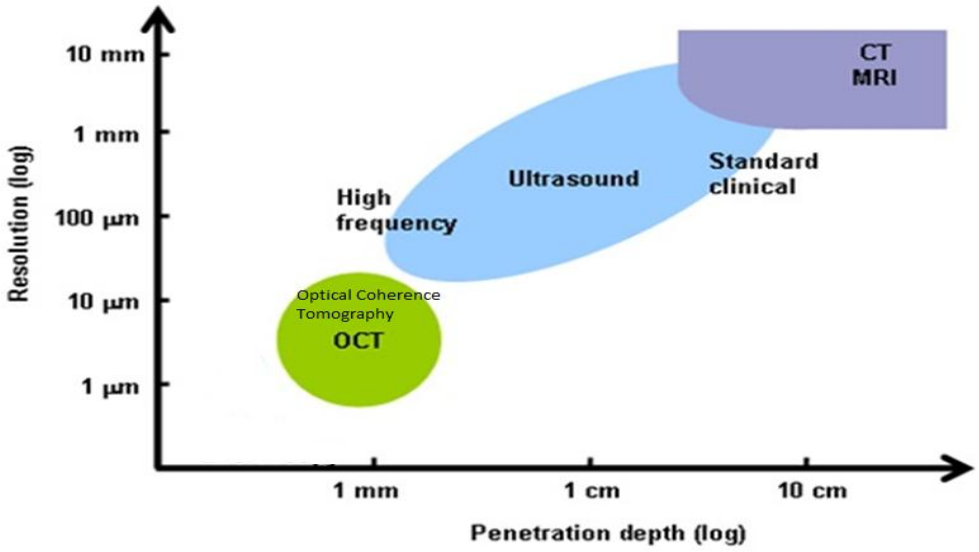

Figure 1-7: Comparison of the resolution and penetration depth of OCT compared to other imaging modalities (adapted from [21]).

Fig 1.7 compares OCT with other imaging modalities. This figure illustrates that the advantage of using OCT is high resolution (10-14 µm) but the disadvantage of using OCT is

the limited penetration depth (2-3 mm). Various groups are trying to make OCT probes to increase the imaging penetration depth. In the next section, the basic principles of OCT will be introduced.

1.4 Basic principles of optical coherence tomography and elastography

Optical Coherence Tomography (OCT) is an optical tomographic imaging technique that shares many similarities to ultrasound imaging despite using light. OCT has several advantages over other imaging modalities, primarily due to its inherently high resolution, which allows for the identification of micron sized morphological tissue structures. This increased resolution comes at the expense of limited imaging penetration depth, which is on the order of a few millimeters. The technology is also flexible and inexpensive. Optical coherence elastography (OCE) measures tissue displacement using OCT and benefits from the high resolution of this imaging technology. OCE is a relatively new elastography technology used to measure biomechanical properties of soft tissue [22]. During OCE, the tissue can be excited internally or externally and statically or dynamically [23]. Methods of creating dynamic compressions include acoustic radiation force (ARF) and low-frequency vibration [24].

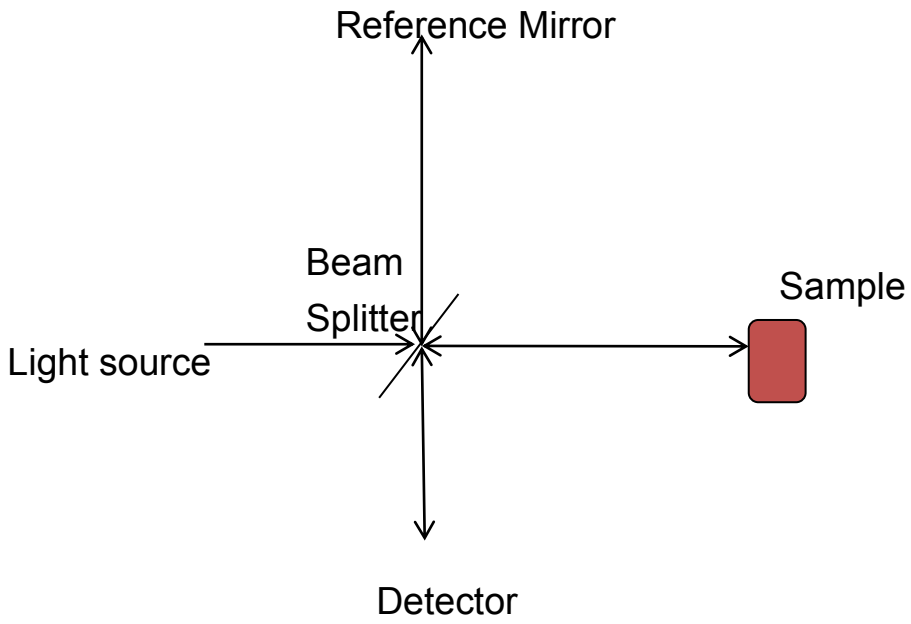

Figure 1-8: Schematic of OCT in simplest form (a Michelson interferometer). The beam splitter can split the light from a low-coherence source into a reference arm and sample arm. Reflections of the sample and reference mirror are recombined into a photodiode detector and the resulting interferometry signal is measured.

The Michelson interferometer takes as an input a beam of light from a source, which is divided into two components at a beam splitter. Fig 1.8 shows an OCT system in its simplest form: a Michelson interferometer in which the beam splitter divides the beam into two equal arms. Half of the light is directed towards the reference arm and a mirror reflects the light back into the detector, and half of the light is directed to the sample arm where a small fraction is backscattered depending on the local sample reflectivity, so that the light interferes

at the detector [25]. However, the broadband light causes interference of the optical fields to occur only when the path lengths of the reference and the sample arm are matched to within the coherence length of the light. This interference signal carries information about the sample reflectivity at a depth determined by the reference path length. The axial resolution is one of the most important parameter in OCT systems since it determines how fine the structures can be resolved in the depth direction. The axial resolution which is determined by coherence length is given by:

$$Lc = 0.44 \frac{\lambda_{\circ}^{2}}{\Delta\lambda} \quad (1.6)$$

The lateral resolution depends on the numerical aperture of the sampling lens and is given by:

$$\Delta x = 1.22 \frac{\lambda}{2NA} \quad (1.7)$$

Where NA is the numerical aperture of the lens. For the OCT system used in this study the lateral resolution was almost 13 μm.

1.4.1 Motion detection using optical coherence tomography

Different techniques can be used to detect the motion using the backscattered data from OCT system. One of the techniques is based on phase maps generated by processing the OCT signals. The backscattered OCT signals can be through to have two frequency components: one of these is the phase modulated carrier frequency while the other is the phase change introduced by the motion of the scattering object. Quadrature demodulation techniques can be used to detect the phase change introduced the motion.

In –phase (I) and quadrature (Q) demodulation: I&Q demodulation are used extensively in signal processing and communication technique.By multiplying the incoming signal by a reference signal and a reference signal shifted in phase by 90^0, two orthogonal vectors are created. These two vectors are the real and imaging components of the incoming signal and referred to as in-phase and quadrature of the incoming signal and are referred to as in-phase and quadrature components respectively.

Signals that are captured by this system are compared to a reference wave and separated into in-phase and quadrature which are represents by S= I+ j Q.

By using these two vectors, the phase can be calculated using a four-quadrant arctangent function where,

φ =Arc tang (Q / I), (1.8)

where Q is imag (OCT_complex), and I is real (OCT_complex). The phase can determine at any points with the range of π to $-\pi$, however, in this study, we used the phase shift, $\Delta\varphi=\varphi_2-\varphi_1$, where φ_2 is the phase when the transducer is on and φ_1 is the phase when is transducer is off [26, 27] and then the phase shift between two successive locations (as explained chapter 2), was calculated. This phase shift was then related to motion within the tissue equivalent phantoms.

1.4.2 OCT elastography to detect shear wave propagation and previous work

Investigators have used OCE to detect tissue motion. ARF was used for the internal mechanical excitation of a sphere embedded in a gelatin phantom, and the phantom deformations were detected with a spectral domain OCT (SD-OCT) system and recorded as M-mode phase images. The displacement of the sphere over time was used for shear modulus

measurements [23]. Tissue velocity and strain measurements have also been obtained via tissue imaged under mechanical loading with a vascular OCE protocol specific to the exploring of tissue biomechanics [28]. Strain responses of tissue phantom undergoing compressive forces have been measured using speckle tracking and SD-OCT methods for detecting small and large deformations [29]. Spectroscopic OCE (S-OCE) has been utilized for frequency-dependent contrast of the displacement amplitude and phase of a silicone phantom, with ex vivo tumor follow-up imaging, in B-mode OCT imaging with applications in pathology [30]. As well, a dynamic SD-OCE technique applied to three-layer silicone tissue phantoms and ex vivo rat tumor tissue has been reported to provide contrast between sample regions with different mechanical properties, thus to mechanically characterize tissue [31]. In vivo three-dimensional OCE has also been implemented to observe elastic properties of superficial skin, which can be utilized for detecting strain rates and contrast useful for pathologists [32,33]. A ring actuator has also been applied to in vivo dynamic OCE to enable excitation and imaging for the same side of the sample, thus providing an alternative for contrast in OCT images [34]. However, in none of the above publications was shear wave propagation directly measured.

We present a novel technique for calculating tissue mechanical properties by propagating shear waves in homogeneous tissue phantoms with ARF, and measuring the shear wave speed and its associated properties with OCT phase maps. The OCT phase maps are acquired with a swept-source OCT (SS-OCT) system. Although SS-OCT systems typically have higher phase noise than SD-OCT(spectral domain)systems , especially at high A-scan rates,

the phase noise of the relatively low speed SS-OCT (8kHz bi-directional) used in these experiments was sufficient to measure phase changes induced by shear wave propagation[35,36]. The dynamic excitation OCE technique uses ARF as the excitation source. In this work, shear modulus measurements of homogeneous tissue equivalent phantoms were made from OCT phase elastograms, without the requirement of measuring displacements of embedded targets as in [23]. We present this methodology as Shear Wave OCE (SW-OCE). This method lays the foundation for future studies of mechanical property measurements of heterogeneous tissue structures, as well as potential research applications in pathology, intravascular studies, US/OCT needle probe imaging, and small animal studies.

There are several advantages for the use of focused ultrasound excitation as the mechanical wave source for inducing shear waves. Advantages include a) the non-invasive nature of ARF excitation to induce deformations in depth in tissue and b) the control of the ultrasound transducer geometrical characteristics and frequency which can induce a wide variety of shear waves (with different frequencies) that would enable probing the tissues at different spatial and temporal scales. This would be much more difficult to achieve using a shaker. Importantly, depending on the mechanical wave driver, consistent coupling of the driver to the tissue is a difficult issue to resolve – and this would result in large result variability.

There are resolution and sensitivity advantages when using ARF excitation and SW-OCE for shear wave propagation detection. SW-OCE utilizes OCT technology, which provides resolution advantages when compared to ultrasound or MRI. OCT provides greater resolution, which allows for the detection of minute deformations in the phantoms that may be critical to the measurement of tissue mechanical properties. It is expected that these maps(

b-map) have much better spatial resolution compared to the shear wave wavelength, in the same way that Fink and colleagues [15] achieve high resolution ultrasound images of shear wave properties using what they term “wave-to-wave” imaging, the difference here being that OCT is used instead of ultrasound imaging to track the shear waves.

The other group described [23] measured the shear modulus based on the ARF displacing a sphere inserted in the phantom to measure the mechanical properties of phantoms. They have experimentally demonstrated an AM-OCE technique that uses dynamic and internal ARF for mechanical excitation However, we have demonstrated, for the first time, a shear wave OCE (SW-OCE) technique that uses ARF for the mechanical excitation directly on the material of interest to measure shear wave propagation. The mechanical excitation produces motion within the phantom that can be used for the estimation of the phantom mechanical properties using OCE. This excitation produces shear waves that propagate perpendicular to the ultrasound beam. The main purpose of this research is to detect the shear wave propagation and directly measure mechanical properties such as shear modulus. Note that the group [23] calculated the shear modulus by using the pushing beam, versus our measurements of shear modulus via the measured shear wave speed. We present the feasibility for OCE measurements of shear wave propagation in homogeneous tissue phantoms as a stepping stone for expanding the research into observing SW-OCE for heterogeneous tissue. In order to eventually move forward with this SW-OCE approach for investigating tissue mechanical properties *in vivo*. The use of homogeneous tissue was only to present this novel technique for measuring shear wave propagation in a simpler setting, but future work will involve heterogeneous tissues to further develop the feasibility of SW-OCE. The method can be used

however in heterogeneous tissues using ultrasound monitoring methods similar to the one used in this research. It should be noted that for clinical ultrasound shear wave imaging, the recent results of the largest clinical breast study ever sponsored by a manufacturer showed that ultrasound specificity increased by 26% with no loss in sensitivity [14]. Their approach uses similar fundamental concepts in the measurement technique. One difference is that in this system we would have to mechanically translate the ARF focal spot by moving the transducer.

1.5 Hypothesis and specific aims

The hypothesis is that OCT can be used to image shear wave propagation in soft tissue with high resolution and be used to measure the mechanical properties of tissue. The goal of this research is to develop shear wave imaging techniques that can image shear wave propagation in homogeneous tissue equivalent phantoms and extract mechanical properties such as the shear modulus the Young's modulus.

The specific aims of this proposed work are to:

a. Design experimental methods to cause tissue deformation caused by an ARF excitation that can be reliably detected using OCT.
b. Obtain the frequency of shear waves produced during ARF excitation based on the M-mode phase maps.
c. Devise methods to measure the shear wave speed based on OCT M-mode and B-mode phase maps.

In this work we determine the reproducibility of shear wave OCE in tissue equivalent phantoms and correlate the mechanical properties measured with this technique with other techniques. By providing high-resolution maps of the mechanical properties of tissue, we hope that this technology can be used to identify changes in the mechanical properties of diseased tissue such as coronary artery disease and cancer.

Chapter 2 Optical coherence elastography measurements of shear wave propagation in homogeneous tissue equivalent phantoms

The result of this work was reported in the following paper

Marjan Razani, Adrian Mariampillai, Cuiru Sun, Timothy W. H. Luk, Victor X. D. Yang, and **Michael C. Kolios "** Feasibility of optical coherence elastography measurements of shear wave propagation in homogeneous tissue equivalent phantoms" (2012)*Biomedical Optics Express*, Vol. 3, Issue 5, pp. 972-980

Feasibility of optical coherence elastography measurements of shear wave propagation in homogeneous tissue equivalent phantoms

Marjan Razani,[1,5] Adrian Mariampillai,[2] Cuiru Sun,[2] Timothy W.H. Luk,[1] Victor X.D. Yang,[1,2,3] and Michael C. Kolios[1,4]

[1]Department of Physics, Ryerson University, Toronto, Canada
[2]Department of Electrical and Computer Engineering, Ryerson University, Toronto, Canada
[3]Division of Neurosurgery, University of Toronto, Toronto, Canada
[4]mkolios@ryerson.ca
[5]mrazani@ryerson.ca

Abstract: In this work, we explored the potential of measuring shear wave propagation using optical coherence elastography (OCE) based on a swept-source optical coherence tomography (OCT) system. Shear waves were generated using a 20 MHz piezoelectric transducer (circular element 8.5 mm diameter) transmitting sine-wave bursts of 400 μs, synchronized with the OCT swept source wavelength sweep. The acoustic radiation force (ARF) was applied to two gelatin phantoms (differing in gelatin concentration by weight, 8% vs. 14%). Differential OCT phase maps, measured with and without the ARF, demonstrate microscopic displacement generated by shear wave propagation in these phantoms of different stiffness. We present preliminary results of OCT derived shear wave propagation velocity and modulus, and compare these results to rheometer measurements. The results demonstrate the feasibility of shear wave OCE (SW-OCE) for high-resolution microscopic homogeneous tissue mechanical property characterization.

OCIS codes: (170.4500) Optical coherence tomography; (170.6935) Tissue characterization.

References and links

1. J. Ophir, S. K. Alam, B. Garra, F. Kallel, E. Konofagou, T. Krouskop, and T. Varghese, "Elastography: ultrasonic estimation and imaging of the elastic properties of tissues," Proc Inst Mech Eng H, **213**(3), 203- 233 (1999).
2. C. Sun, B. Standish, and V. X. D. Yang, "Optical coherence elastography: current status and future applications," JBO, **16**(4), 043001 (2011).
3. J. M. Schmitt, "OCT elastography: imaging microscopic deformation and strain of tissue," Opt. Express, **3**(6), 199-211 (1998).
4. X. Liang, M. Orescanin, K. S. Toohey, M. F. Insana, and S. A. Boppart, "Acoustomotive optical coherence elastography for measuring material mechanical properties," Opt. Letters, **34**(19), 2894-2896 (2009).
5. J. F. Greenleaf, M. Fatemi, and M. Insana, "Selected methods for imaging elastic properties of biological tissues," Annu. Rev. Biomed. Eng, **5**, 57-78 (2003).
6. M. Fatemi and J. F. Greenleaf, "Application of radiation force in noncontact measurements of the elastic parameters," Ultrason. Imaging, **21**(2), 147-154 (1999).
7. M. E. Hachemi, S. Calle, and J. P. Remenieras, "Transient displacement induced in shear wave elastography: Comparison between analytical results and ultrasound measurements," Ultrasonics, **44**(22), 221-225 (2006).

8. L. Ostrovsky, A. Sutin, Y. Il'inskii, O. Rudenko, and A. Sarvazyan, "Radiation force and shear motions in inhomogeneous media," J. Acoust. Soc. Am, **121**(3), 1324-1331 (2007).

9. M. L. Palmeri, S. A. McAleavey, K. L. Fong, G. E. Trahey, and K. R. Nightingale, "Dynamic mechanical response of elastic spherical inclusions to impulsive acoustic radiation force excitation," IEEE Trans. Ultrason., Ferroelectr., Freq. Control, **53**(11), 2065-2079 (2006).

10. W. F. Walker, F. J. Fernandez, and L. A Negron, "A method of imaging viscoelastic parameters with acoustic radiation force," Phys.Med. Biol, **45**(6), 1437-1447 (2000).

11. K. Nightingale, M. S. Soo, R. Nightingale, and G. Trahey, "Acoustic radiation force impulse imaging: In vivo demonstration of clinical feasibility," Ultrasound Med Biol, **28**(2), 227-235 (2002).

12. K. R. Nightingale, R. W. Nightingale, D. L. Stutz, and G. E. Trahey, "Acoustic radiation force impulse imaging of in vivo Vastus Medialis muscle under varying isometric load," Ultrasonic Imaging, **24**,100-108 (2002).

13. M. Fatemi and J. F. Greenleaf, "Ultrasound-stimulated vibro-acoustic spectrography," Science, **280**(5360), 82-85 (1998).

14. K. Nightingale, M. Palmeri, and G. Trahey, "Analysis of contrast in images generated with transient acoustic radiation force," Ultrasound Med. Biol, **32**(1), 61-72 (2006).

15. R.C. Chan, A.H. Chau,W.C. Karl, S. Nadkarni, A.S. Khalil, N. Iftimia, M. Shishkov, G.J. Tearney, M.R. Kaazempur-Mofrad, and B. E. Bouma, "OCT-based arterial

elastography: robust estimation exploiting tissue biomechanics,"Opt. Express,**12**(19),4558-4572(2004).

16. S. J. Kirkpatrick, R. K. Wang, and D. D. Duncan, "OCT-based elastography for large and small Deformations," Opt. Express,**14**(24) ,11585-11597(2006).

17. S. G. Adie, X. Liang, B. F. Kennedy, R. John, D. D. Sampson, and S. A. Boppart, " Spectroscopic optical coherence elastography," Opt. Express,**18**(25),25519-25534(2010).

18. X. Liang, S. G. Adie, R.John, and S. A. Boppart, "Dynamic spectral-domain optical coherence elastography for tissue characterization," Opt. Express,**18**(13),14183-14190(2010).

19. B. F. Kennedy, X. Liang, S. G. Adie, D. K. Gerstmann, B. C. Quirk, S. A. Boppart, and D.D. Sampson1, " *In vivo* three-dimensional optical coherence elastography," Opt. Express,**19**(7),6623-6634(2011).

20. X. Liang and S.A. Boppart, Biomechanical properties of in vivo human skin from dynamic optical coherence elastography,' T-BME," **57**(4), 953-959(2010).

21. B.F. Kennedy, T. R. Hillman, R. A. McLaughlin, B. C. Quirk, and D. D. Sampson, "*In vivo* dynamic optical coherence elastography using a ring actuator," Opt. Express,,**17**(24),21762-21772(2009).

22. S. H. Yun, G. J. Tearney, J. F. de Boer, and B. E. Bouma, "Motion artifacts in optical coherence tomography with frequency-domain ranging," Opt. Express,**12**(13),2977-2998(2004).

23. A. Mariampillai, B. A. Standish, N. R. Munce, C. Randall, G. Liu, J. Y. Jiang, A. E. Cable, I. A. Vitkin, and V. Yang , "Doppler optical cardiogram gated 2D color flow imaging at 1000 fps and 4D in vivo visualization of embryonic heart at 45 fps on a swept source ," Opt. Express, **15**(4), 1627-1638 (2007).

24. J. Bercoff, M. Tanter, and M. Fink, "Supersonic shear imaging: A new technique for soft tissue elasticity mapping," IEEE Trans. Ultrason., Ferroelectr., Freq. Control, **51**(4), 396 - 409 (2004).

25. K. Nightingale, S. McAleavey, and G. Trahey, "Shear wave generation using acoustic radiation force: In vivo and ex vivo results,"Ultrasound Med. Biol, **29**(2), 1715-1723 (2003).

26. M. L. Palmeri, S. A. McAleavey, G. E. Trahey, and K. R. Nightingale, "Ultrasonic tracking of acoustic radiation force-induced displacements in homogeneous media," IEEE Trans. Ultrason., Ferroelectr., Freq. Control, **53**(7), 1300–1313 (2006).

27. G. F. Pinton and G. E. Trahey, "Continuous delay estimation with polynomial splines," IEEE Trans. Ultrason., Ferroelectr., Freq. Control, **53**(11), 2026-2035 (2006).

28. J. McLaughlin and D. Renzi, "Shear wave speed recovery in transient elastography and supersonic imaging using propagating fronts,"Inverse Probl, **22**, 681-706 (2006).

29. J. McLaughlin and D. Renzi, "Using level set based inversion of arrival times to recover shear wave speed in transient elastography and supersonic imaging," Inverse Probl, **22**, 707-725 (2006).

30. M. L. Palmeri, M. H. Wang, J. J. Dahl, K. D. Frinkley, and K. R. Nightingale, "Quantifying hepatic shear modulus in vivo using acoustic radiation force," Ultrasound Med. Biol, **34**(4), 546-558 (2008).

31. A. Karpiouk, S. Aglyamov, Y. Ilinskii, E. Zabolotskaya, and S. Emelianov, "Assessment of shear modulus of tissue using ultrasound radiation force acting on a spherical acoustic inhomogeneity," IEEE Trans. Ultrason., Ferroelectr., Freq. Control, **56**(11), 2380 - 2387 (2009).

32. A. P. Sarvazyan, O. V. Rudenko, S. D. Swanson, J. B. Fowlkes, and S. Y. Emelianov, "Shear wave elasticity imaging: A new ultrasonic technology of medical diagnostics," UMB, **24**(9), 1419-1435 (1998).

33. M. Orescanin, "Complex shear modulus reconstruction using ultrasound," Thesis, University of Illinois at Urbana-Champaign,1-185 (2010).

34. W. A. Berg, D. O. Cosgrove, C. J. Doré, F. K. W. Schäfer, W. E. Svensson, R. J. Hooley, R. Ohlinger, E. B. Mendelson, C. B-Maestro, M. Locatelli, C. Tourasse, B. C. Cavanaugh, V. Juhan, A. T. Stavros, A. Tardivon, J. Gay, J. P. Henry, and C. C-Bacrie,"Shear-wave elastography improves the specificity of breast US: the be1 multinational study of 939 masses ," *Radiology*, **262**(2),435-449(2012).

35. M. Fatemi and J. F. Greenleaf, "Vibro-acoustography: an imaging modality based on ultrasound-stimulated acoustic emission," Proc. Natl. Acad. Sci. USA, **96**(12), 6603-6608 (1999).

36. S. Chen, M. Fatemi and J. F. Greenleaf, "Quantifying elasticity and viscosity from measurement of shear wave speed dispersion," J. Acoust. Soc. Am, **115**(6), 2781-5 (2004).

37. K. R. Nightingale, R. Bentley, and G. E. Trahey, "Observations of tissue response to acoustic radiation force: opportunities for imaging", Ultrasonic Imaging, **24**, 100-108 (2002).

38. Y. Yamakoshi, J. Sato and T. Sato, "Ultrasonic imaging of internal vibration of soft tissue under forced vibration," IEEE Trans. Ultrason., Ferroelectr., Freq. Control, **37**(2), 45-53 (1990).

39. S. Chen, M. Fatemi and J. F. Greenleaf, "Remote measurements of material properties from radiation force including vibrations of an embedded sphere," J. Acoust. Soc. Am, **112**(3), 884-889 (2002).

40. E. E. Konofagou and J. Ophir , " A new elastographic method for estimation and imaging of lateral strains, corrected axial strains and poison's ratios in tissues," Ultrasound in Med. & Biol ,**24**(8), 1183-1199(1998).

41. C. Amador, M. W. Urban, S. Chen, Q. Chen, K-N. An, and J. F. Greenleaf, "Shear elastic modulus estimation from indentation and SDUV on gelatin phantoms" IEEE Trans. Biomed.Eng, **58**(6), 1706 - 1714 (2011).

42. C. Li, G. Guan, X. Cheng, Z. Huang, and R. K. Wang, " Quantitative elastography provided by surface acoustic waves measured by phase-sensitive optical coherence tomography," Opt. Letters, **37**(4), 722-724(2012).

1. Introduction

Elastography is a method of generating stiffness and strain images of soft tissues for diagnostic purposes [1]. An imaging modality is used to detect tissue deformation behaviors under static or dynamic load and presents the resulting images as elastograms. Elastograms contain information about local variations of stiffness inside a region of interest, as well as additional clinical information such as the identification of suspicious lesions, the diagnosis of various disease states, and the monitoring of the effectiveness of treatments. Different imaging modalities such as ultrasound (US) imaging or magnetic resonance imaging (MRI) can be used to measure tissue displacements and estimate the resulting tissue mechanical properties [2]. Drawbacks of MRI include cost, long clinical wait times, and technological complexity. As well, both US and MRI have spatial resolutions in the order of 0.1-1 mm, which is insufficient for detecting small and subtle elastic variations in tissues, such as in small tumors and atherosclerotic plaques. Optical coherence tomography (OCT) is an optical tomographic imaging technique that shares many similarities to ultrasound imaging despite using light. OCT has several advantages over other imaging modalities, primarily due to its inherently high resolution, which allows for the identification of micron sized morphological tissue structures. Although the improved resolution comes at the expense of limited imaging penetration depth to the order of a few millimeters, OCT equipment is inexpensive and its interchangeable components enable experiment-specific flexibility. Optical coherence elastography (OCE) is a relatively new elastography technology that uses OCT to measure tissue displacement and biomechanical properties of soft tissues [3]. During OCE, tissues can

be excited internally or externally, as well as statically or dynamically [4]. Methods for creating dynamic compressions include acoustic radiation force (ARF) and low-frequency vibrations with a needle [5].

ARF excitation for producing transient excitations has been implemented to assess the mechanical properties of tissues. ARF imaging is used in general elasticity imaging methods [6-10], for the characterization of lesions [11, 22], muscle screening [12], and imaging of the calcification of arteries [13]. Most investigators are exploring methods to measure the tissue mechanical properties using external excitation of the tissue [14]. ARF has also been used for the internal mechanical excitation of a sphere embedded in a gelatin phantom, with phantom deformations detected with a spectral domain OCT (SD-OCT) system and recorded as M-mode phase images and then the displacement of the sphere over time was used for shear modulus measurements. [4]. Tissue velocity and strain measurements have been obtained via tissue imaged under mechanical loading with a vascular OCE protocol specific to the exploring of tissue biomechanics [15]. Strain responses of tissue phantom undergoing compressive forces have been measured using speckle tracking and SD-OCT methods for detecting small and large deformations [16]. Spectroscopic OCE (S-OCE) has been utilized for frequency-dependent contrast of the displacement amplitude and phase of a silicone phantom, with ex vivo tumor follow-up imaging, in B-mode OCT imaging with applications in pathology [17]. As well, a dynamic SD-OCE technique applied to three-layer silicone tissue phantoms and ex vivo rat tumor tissue has been reported to provide contrast between sample regions with different mechanical properties, thus to mechanically characterize tissue

[18]. In vivo three-dimensional OCE has also been implemented to observe elastic properties of superficial skin, which can be utilized for detecting strain rates and contrast useful for pathologists [19,20]. A ring actuator has also been applied to in vivo dynamic OCE to enable excitation and imaging for the same side of the sample, thus providing an alternative for contrast in OCT images [21].

We present a novel technique for calculating tissue mechanical properties by propagating shear waves in homogeneous tissue phantoms with ARF and measuring the shear wave speed and its associated properties with OCT phase maps. The OCT phase maps are acquired with a swept-source OCT (SS-OCT)system. Although SS-OCT systems typically have higher phase noise than SD-OCT systems , especially at high A-scan rates, the phase noise of the relatively low speed SS-OCT (8kHz bi-directional) used in these experiments was sufficient to measure phase changes induced by shear wave propagation[22,23]. The dynamic excitation OCE technique uses ARF as the excitation source. There are several ways that shear wave speed can be measured. These methods include the inversion of the Helmholtz Equation, which characterizes the shear wave propagation [24, 25], using algorithms that measure lateral time for peak-to-peak displacements [29], tracking the displacement field jitters that are associated with shear waves [26, 27], and using a variety of correlation-based algorithms [28, 29]. The speed of shear waves that propagate in soft tissues is directly related to the shear modulus of the material [30, 31]. Traditional compression wave imaging methodologies, such as US, provide measurements based on the tissue bulk modulus, which is confined to a relatively small range for soft tissues. The shear modulus for soft biological

tissues actually span a much larger range compared to the bulk modulus by several orders of magnitude [32, 33]. The use of the shear modulus as a cancer biomarker has been recently demonstrated using ultrasonic techniques [34]. In this work, shear modulus measurements of homogeneous tissue equivalent phantoms were made from OCT phase elastograms, without the requirement of measuring displacements of embedded targets. We present this methodology as Shear Wave OCE (SW-OCE). This method lays the foundation for future studies of mechanical property measurements of heterogeneous tissue structures, as well as potential research applications in pathology, intravascular studies, US/OCT needle probe imaging, and small animal studies.

2. Acoustic radiation force

Acoustic radiation force (ARF) is produced by a change in the energy density of the incident acoustic field [35, 36]. The acoustic radiation force is generated by the transfer of momentum from the acoustic wave to the tissue. This force is applied in the direction of the longitudinal wave propagation and the magnitude of the force can be approximated by:

$$F = \frac{2\alpha I}{C}. \qquad (1)$$

where F, kg/(s ^{2} cm ^{2}), is the acoustic radiation force, C (m/s) is the speed of sound in the medium, α (Np/m) is the absorption coefficient of the medium and I (W/cm^2) is the temporal average intensity at a given spatial location [37]. Fig. 1 shows the principle of shear wave generation. Shear waves can be generated by using a focused impulse generated by an ultrasound transducer. The impulse creates a displacement in the direction of ultrasonic beam propagation which is largest at the transducer focus. After the impulse the material relaxes

back to its original state producing a shear wave. The shear wave propagates in the direction perpendicular to the direction of the focused US propagation.

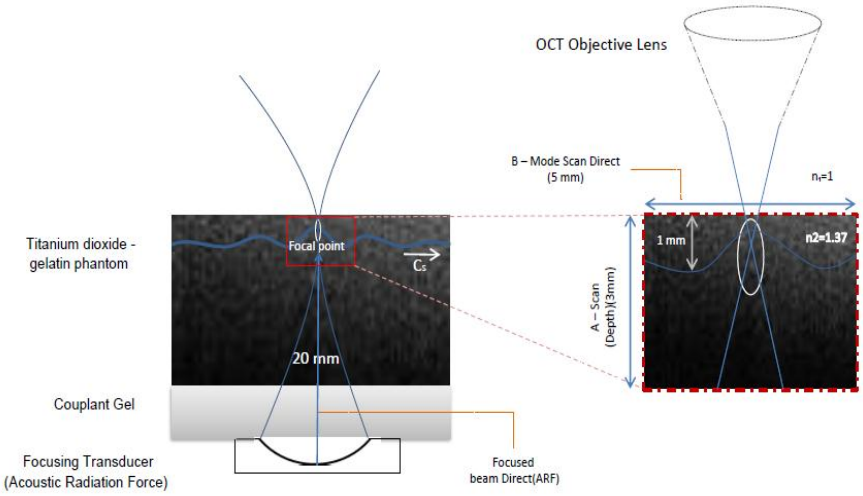

Fig. 1. Using a focused ARF impulse generated by a transducer, shear waves can be produced at the focal point. We detect the shear wave that travels within the titanium dioxide-gelatin phantom in the direction indicated by the white arrow labeled C_s. The transducer focal depth for this study was 20 mm. B-mode OCT images were taken at the focal point for phase map analysis.

2.1 Shear moduli and wave propagation

By using the Voigt model for a homogenous medium, the shear wave speed C_s can be related to the shear modulus μ_1, shear viscosity μ_2, shear wave angular frequency ω, and tissue density ρ as follows [36, 38, 39]:

$$C_S(\omega) = \sqrt{2(\mu_1^2 + \omega^2 \mu_2^2) / \rho(\mu_1 + \sqrt{\mu_1^2 + \omega^2 \mu_2^2})}. \quad (2)$$

Experimentally, the displacements of shear waves at each tracking location are calculated with a speckle-tracking algorithm based on the OCT phase maps generated. The shear wave speed could be calculated using $\Delta\varphi$ and Δr measurements obtained from the measured phase shift, and the distance between the two tracking locations, respectively. The shear wave speed can be calculated using the following Eq.:

$$C_S(\omega) = \frac{\omega \Delta r}{\Delta \varphi}. \quad (3)$$

where $\omega = 2\pi f$, $\Delta\varphi$ *is* the phase shift, and Δr *is* the distance between the two tracking locations. The shear wave frequency (f) is dependent on several factors, the most dominant of which is the beam width of the excitation transducer.

The Young's modulus and shear modulus are also important to defining the tissue mechanical properties. They can be calculated using the following Eq. (which assumes an isotropic homogeneous medium):

$$C_s = \sqrt{\frac{\mu}{\rho}}. \quad (4)$$

and

$$E = 2(1+\nu)\mu \approx 3\mu = 3C_S{}^2\rho. \quad (5)$$

Where ν, μ, E represents the Poisson's ratio, shear modulus and Young's modulus, respectively. Here we make the assumption that soft tissues are close to incompressible, with a constant Poisson's ratio of close to 0.5 (0.495)[40].

3. Materials and methods

In this study, we present a dynamic excitation OCE technique using ultrasound ARF as the excitation source. A custom SS-OCT system was used in this study. The laser had a center wavelength of a 1310 nm, a bandwidth of ~110 nm, and an A-scan rate of 8 kHz. The lateral resolution was approximately 13μm in the samples. ARF(internal mechanical excitation) was applied using a 20 MHz, circular, 8.5 mm diameter piezoelectric transducer element (PZT, f-number 2.35) transmitting sine-wave bursts of 400 μs. The OCT images were taken with an existing swept-source system. B-mode images were taken of a titanium dioxide-gelatin phantom that was 5 mm in length. The OCT image A-scan depth was 3 mm. The focal point of the transducer used for the ARF experiments was 20 mm from the transducer surface and the focal spot was located about 1 mm below the top surface of the gelatin phantom. Fig. 1 shows that M-mode images were taken along the y-direction, the direction of the ARF beam.

Shear waves predominantly propagate radially outwards from the focal point, perpendicular to the direction of the ARF beam (the shear waves propagate along the x-axis). The PZT element

push sequence was synchronized with the OCT imaging triggering system. The US depth of field was 2.94 mm, with US focus of 20 mm. The full width at half maximum was calculated to be 246 μm.

The phantom in this study consisted of gelatin mixed with titanium dioxide, which provided uniform acoustic and optical scattering. Gelatin powder (Type B, Fisher Scientific, G7-500) and distilled water were heated in a water bath at 60−65 ^{0}C for one hour and periodically stirred. Two tissue phantoms with different gelatin concentrations were prepared (Phantom 1: 14%, Phantom 2: 8%). When the phantom samples cooled to 45 ^{0}C, 0.1% weight by weight titanium dioxide (Sigma-Aldrich, Titanium(IV) oxide nanopowder, <25 nm particle size, 99.7% trace metals basis) was added and thoroughly mixed. The phantom solution was poured into rectangle molds (20 mm height) and allowed to congeal. The titanium dioxide was used as a scattering agent. Fig. 2 shows the schematic of the Acoustic Radiation Force-Optical Coherence Elastography (ARF-OCE) setup.

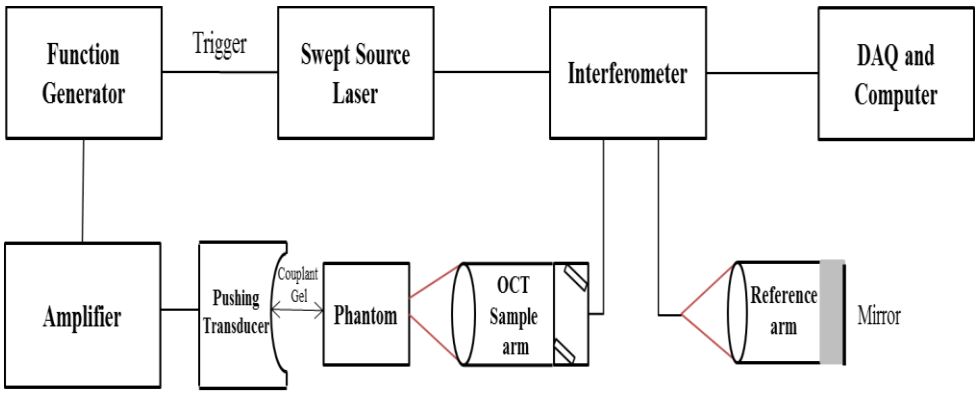

Fig 2. The ARF-OCE experimental setup consisted of the existing SS-OCT system, a titanium dioxide-gelatin phantom, a focused transducer (20 MHz, f-number 2.35), an amplifier and a function generator (Agilent 33250A 80 MHz, Function / Arbitrary Waveform Generator) synchronized with the SS-OCT system.

The OCT signals from the phantoms were used for the measurement of the shear wave speed and mechanical properties. The US "push" transducer was synchronized with the OCT imaging system. The phase analysis was applied to B-mode and M-mode OCT images, which were obtained while the US transducer was generating the "push" in the phantom. A fast Fourier transform was performed on the OCT data, and phase maps of the phantom under US loading were generated and are directly related to the ARF induced displacement in the phantom**.**

Independent measurements of the mechanical properties of the phantom were made using a rheometer. Material properties of the same gelatin gels imaged using SW-OCE (14% w/w and 8% gelatin concentrations) were tested in a parallel-plate shear rheometer in oscillatory mode using a Physica MCR 301 rheometer (Anton Paar GmbH, Graz, Austria) equipped with Peltier plate temperature control unit (P-PTD 200). The parallel plate measuring geometry (PP 25/TG) with a diameter of 25mm was used. The frequency dependent elastic and viscous moduli, G' and G'', were measured for the 1 hour aged samples at 25 °C for frequencies ranging from 10^{-1} Hz to10^{2} Hz. To avoid sample drying, the measuring geometry was covered with a solvent trap containing a moist strip of paper tissue. Preceding each measurement, the temperature of the Peltier plate was set at 10 °C and the mixed hot biopolymer solution was poured directly onto the cold plate. The quenched sample rapidly transformed to a gel after

which the temperature of the rheometer cell was raised from 10 °C to 25°C at a rate of 6 °C min^{-1}. The upper cone was then lowered onto the sample to an operating gap width (1 mm) and the sample was trimmed and held at 25 °C for 10 minutes. Using this standard thermal treatment, the conventional gel state condition was readily satisfied for all samples. After thermal treatment, rheological measurements at 25 °C were performed. To obtain the moduli at the dominant frequency of the shear waves generated in the SW-OCE experiments, the rheometer shear modulus versus frequency data had to be extrapolated to the value of interest.

4. Results and conclusion

OCT images of the titanium dioxide-gelatin phantom were taken with the SS-OCT system and shown in Fig. 3. B-mode and M-mode images of the phantom, as well as their respective phase maps provide information that is required to calculate distance, the phase shift between two locations and the shear wave frequency.

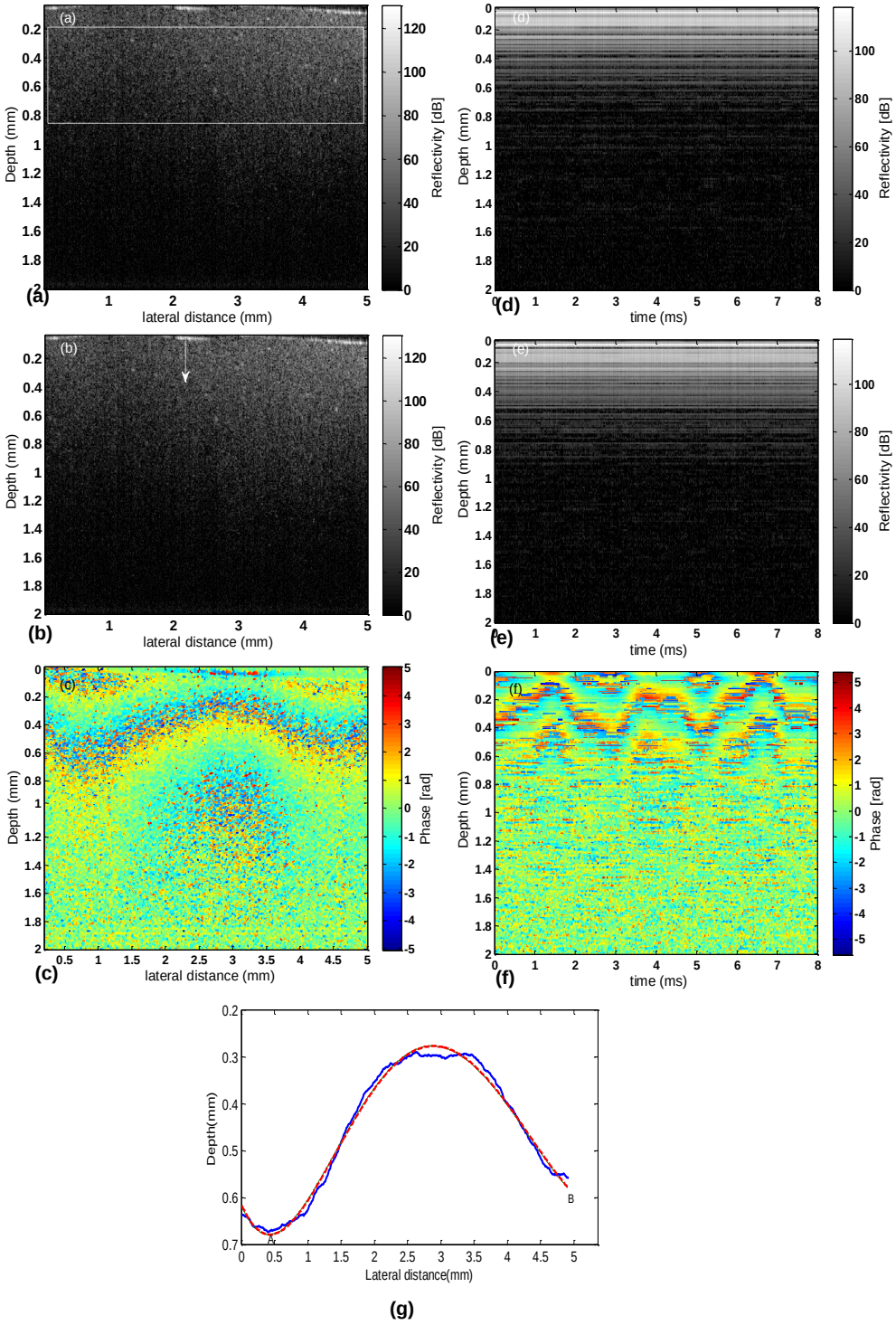
(a)
Depth (mm)
lateral distance (mm)
Reflectivity [dB]
(d)
time (ms)
(b)
(e)
(c)
Phase [rad]
(f)
(g)
Depth(mm)
Lateral distance(mm)
A
B

Fig.3. B-mode OCT images (a and b) and the corresponding B-mode phase map (c) of the titanium dioxide-gelatin phantom (14%) were taken with the SS-OCT system. The dashed box(a) represents the location of the superimposed fitted sine wave observed in the phase map. The white arrow(b) indicates the position where the M-mode OCT images (d and e),with the ARF on and off, respectively, were acquired and synchronized with the OCT swept-source wavelength sweep. The B-mode phase map of the phantom was used to measure Δr and $\Delta\varphi$ for the calculation of the shear wave speed. The color scale represented the change of the phase value (radians). The M-mode phase map (f) from this phantom was used to calculate the shear wave frequency. To better illustrate the calculation of Δr , MATLAB was used to to plot an isophase curve which now shows the experimental data (blue). The red curve is a best fit with a polynomial (g).

By measuring the time difference between successive troughs in the M-mode dataset of Fig. 3(f), the dominant frequency of the shear wave was calculated to be approximately 266 Hz (for both the phantoms). The shear wave group speed was then calculated by using the Δr and $\Delta\varphi$ obtained from Fig. 3(c, g), which depicts the distance between the two successive locations and the measured phase shift, respectively. Two successive locations can be chosen at a particular depth z (in this work we chose z= 0.6mm). At these two locations in the image, phase values are retrieved. The calculation of $\Delta\phi$ involves the measurements of the two phase

values at the aforementioned two locations, which are then used in eq. 3 to calculate the shear wave group velocity. Another way to illustrate a "snapshot" of the shear wave is to plot an isophase curve which was generated by averaging the phase value between depths from 0.25 mm to 0.7 mm Fig. 3(g). These values were then used in Eq. (3) to calculate the shear wave speed. The shear wave speeds for the 14% and 8% gelatin-titanium dioxide phantoms were 2.24 ± 0.06 m/s and 1.49 ± 0.05 m/s, respectively, and reported in Table. A. The average values and standard deviations were calculated from 10 different pairs of locations in the phase maps for all calculations of Δr and $\Delta \varphi$.

The Young's moduli and shear moduli were also calculated using the above results. The measured density ρ of the phantom samples was 1050 kg/m^3. Table. A summarizes the Young's moduli and shear moduli for both phantoms. The shear modulus estimated using SW-OCE for Phantom 1 (14%) was 5.3±0.2 kPa and for Phantom 2 (8%) was 2.3±0.1 kPa. The errors for the SW-OCE results represent the standard deviation. As expected, the values of the Young's moduli and shear moduli were greater for the phantom with the higher concentration of gelatin [41]. The shear moduli of both phantoms calculated using SW-OCE was compared to the shear moduli of the same two phantoms measured by the rheometer in Table. A. The errors for the rheometer results represent the standard deviations.

Table (A): The mechanical properties of the phantoms.

Samples	**Shear wave speed (C_s, m/s)**	**Shear modulus (μ, kPa)**	**Young modulus (E, kPa)**
Phantom 1 (14%)	2.24±0.06	5.3±0.2	15.8±0.6
Rheometer		4.93±0.05	
Phantom 2 (8%)	1.49±0.05	2.3±0.1	7.0±0.3
Rheometer		2.06±0.09	

In summary, we have demonstrated, for the first time, a SW-OCE technique that uses ARF for mechanical excitation of a homogeneous gelatin phantom to measure shear wave propagation. The mechanical excitation produces motions within the phantom that can be used for the estimation of mechanical properties using SW-OCE. This excitation produces shear waves that propagate perpendicular to the US beam. The close proximity of the transducer focus to the surface of the phantom suggests that the surface (Rayleigh) waves were produced [42]. The discrepancy between the values provided by the rheometer and the SW-OCE technique may be related to the extrapolation required from the rheometer data to obtain the values of the shear modulus at 266 Hz and the fact that the SW-OCE technique, as implemented, is more sensitive to the shear wave group velocity, whereas the shear modulus from the rheometer is reported at one frequency. Possible *in vivo* clinical applications of this method of SW-OCE include pathology, intravascular studies, US/OCT catheter imaging, and

small animal studies due to the potential for measuring mechanical properties within tissues as a disease assessments.

Acknowledgments

Marjan Razani is supported by an Ontario Graduate Scholarship (OGS). This work is funded in part by the Canada Research Chairs program (awarded to Drs. V.X.D. Yang and M. C. Kolios), the Natural Sciences and Engineering Research Council of Canada (NSERC discovery grant 216986-07) and Canada Foundation for Innovation. We would like to thank Dr. Mathias Fink, Dr. Hassan Firoozmand, Dr. Dérick Rousseau and Arthur Worthington for their contributions and discussions.

Chapter 3 Discussion and Future work

3.1 Discussion

This thesis presents a newly developed method to measure the mechanical properties of phantoms using optical coherence tomography. To achieve this, the acoustic radiation force produced by focused ultrasound beams was used to produce shear waves. The phantom motion induced by the shear waves was detected using optical coherence tomography and phase sensitive motion algorithms. Using this technique, mechanical properties of the phantoms were measured such as the shear modulus and Young's modulus. Results of these measurements were compared to rheometer measurements and demonstrated reasonable agreement (Table A, Chapter 2). The same phantoms were used for the rheometer and SW-OCE testing. The discrepancy between the values provided by the rheometer and the SW-OCE technique may be related to the extrapolation required from the rheometer data to obtain the values of the shear modulus at 266 Hz and the fact that the SW-OCE technique, as implemented, is more sensitive to the shear wave group velocity, whereas the shear modulus value from the rheometer is reported at one frequency, as shown in Table A, Chapter 2. Note that we used phantoms of different concentrations to show that the patterns observed are related to the phantom mechanical properties (Appendix A). This is the first time for which such mechanical properties of phantoms were measured directly by using Optical Coherence Tomography without the need to embed objects in the tissue or phantom and trace the motion of the object.

OCT provides greater spatial and phase resolution, which allows for the detection of minute deformations in the phantoms that may be critical to the measurement of tissue mechanical properties. The spatial resolution of mechanical property maps will depend on whether reliable phase difference measurements between two locations can be made with SW-OCE. It is expected that these maps have much better spatial resolution compared to the shear wave wavelength, in the same way that Fink and colleagues [15] achieve high resolution ultrasound images of shear wave properties using what they term “wave-to-wave” imaging, the difference here being that OCT is used instead of ultrasound imaging to track the shear waves. The spatial and phase resolution advantages of OCT compared to ultrasound are expected to provide mechanical property maps with greater spatial and contrast resolution.

The OCT phase maps were acquired with a swept-source OCT (SS-OCT) system. Although SS-OCT systems typically have higher phase noise than SD-OCT systems, especially at high A-scan rates, the phase noise of the relatively low speed SS-OCT (8kHz bi-directional) used in these experiments was sufficient to measure phase changes induced by shear wave propagation. The OCT system is very sensitive as even very small vibrations or electronics device noise will effect on the phase stability. To minimize this effect, the flooding table was set up by using compressor in during all experiments.

3.2 Future work

The beam width of the excitation dictates the frequency content of the shear wave

produced, which is affected by the geometrical focusing (f-number) and to some degree by the frequency of the excitation. Strong focusing also limits the excitation region to smaller tissue regions, which is an important consideration for heterogeneous tissues. In future work different transducers with different f-numbers will be used. The design of such transducers will depend on the application envisioned and the scales of the heterogeneities that need to be imaged (such as atherosclerotic plaques). The further testing for heterogeneous phantoms as well as biological samples is required to fully demonstrate feasibility of SW-OCE to measure shear wave propagation in heterogeneous tissues. Proof of principle experiments presented in this thesis on simple homogenous phantoms with known and well controlled properties is the first step in this process.

This newly developed technique has many potential applications, including identifying the mechanical properties of tissue and identifying changes in the mechanical properties associated with artery disease and cancer. Other possible in vivo clinical applications of this method of SW-OCE include tissue pathology, US/OCT catheter imaging and small animal studies due to the potential for measuring mechanical properties within tissues for disease assessment. This method of SW-OCE for investigating tissue mechanical properties via shear wave measurements will be explored next *in vitro* and *in vivo* for atherosclerotic vascular tissues for which large contrast in the shear modulus is expected between the lipid core of an atherosclerotic plaque and the fibrous plaque. It should be noted that for clinical ultrasound shear wave imaging, the recent results of the largest clinical breast study ever sponsored by a manufacturer for the detection of breast cancer (the multinational, multicenter "Breast Elastography 1 (BE1)" study) showed that ultrasound specificity increased by 26% with no

loss in sensitivity [14]. This illustrates the relevance of this mechanical property as a cancer biomarker. The approach adapted in this paper uses similar fundamental concepts in the measurement technique.

3.3 Conclusions

In summary, we have demonstrated, for the first time, a SW-OCE technique that uses ARF for mechanical excitation of a homogeneous gelatin phantom to measure shear wave propagation. The mechanical excitation produces motions within the phantom that can be used for the estimation of mechanical properties using SW-OCE. A comparison of the mechanical properties of two different tissue equivalent phantoms measured using this novel method with rheometer measurements demonstrated good agreement, illustrating the potential of the technique for the mechanical characterization of tissues.

Appendix : Comparing the results of the 8% vs 14% Gelatin Phantoms

OCT images of the titanium dioxide-gelatin phantom were taken with the SS-OCT system and shown in Fig. 3 in Chapter 2. B-mode and M-mode images of the phantom, as well as their respective phase maps provide information that is required to calculate distance, the phase shift between two locations and the shear wave frequency.

In this study we used phantoms with two different concentrations of gelatin. The results were reported in Chapter 2. In this appendix, we compare the results of the 8% vs 14% Gelatin phantoms for both the B-mode and M-mode images to illustrate the change in B-mode images but similar M-mode images for the two phantoms. Figure A shows the results

	14% concentration gelatin phantom/titanium dioxide	**8% concentration gelatin phantom/titanium dioxide**
B-mode phase map	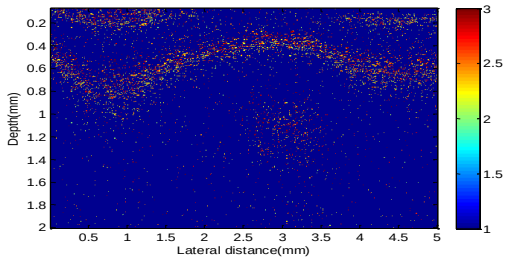	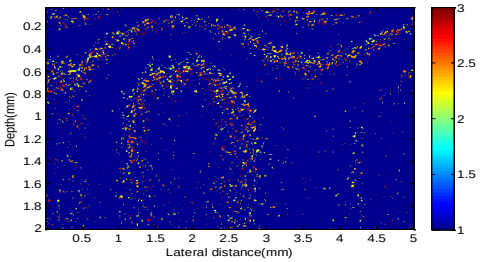
M-mode phase map	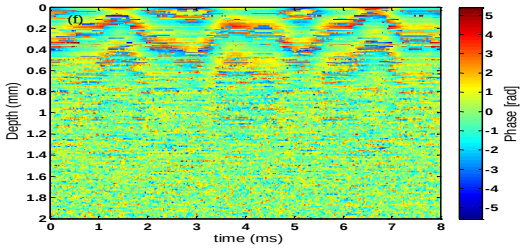	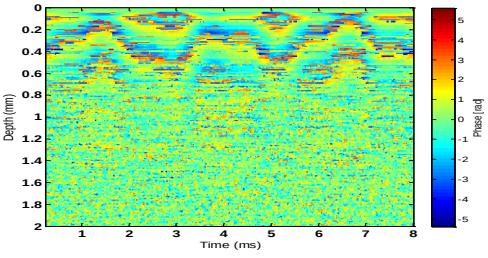

of the B- mode image and M-mode image for 8% (right panel) and 14% (left panel) gelatin phantoms.

Figure A.1: Comparison of the B-Mode (top panel) and M-mode (bottom panel) phase maps of the 14% (left panel) and 8% (right panel) concentration gelatin phantom/titanium dioxide phantoms.

The shear wave group speed was then calculated by using B-mode and M-mode phase map. The Young's moduli and shear moduli were also calculated using shear wave speed. The shear modulus estimated using SW-OCE for Phantom 1 (14%) was 5.3±0.2 kPa and for Phantom 2 (8%) was 2.3±0.1 kPa. It should be noted that the frequency of shear wave is the same for both phantoms (14% and 8%, Figure A.1, M-mode phase map) but the wavelength of the shear wave is not the same (Figure A.1, B-mode phase map). It should be further noted that M-mode images are generated by fixing the incident beam at one position on the phantom and acquiring axial scans over time which the x-axis represents time (Fig 3,d,e,f ,the scale time shows only forward time) and y-axis represents phantom depth, so to calculate the frequency, the time should be multiplied by a factor of two.

Bibliography

1. C. Amador, M. W. Urban, S. Chen, Q. Chen, K-N. An, and J. F. Greenleaf, "Shear elastic modulus estimation from indentation and SDUV on gelatin phantoms" IEEE Trans. Biomed.Eng, **58**(6), 1706 - 1714 (2011).
2. http://www.tjhsst.edu/~jlafever/wanimate/Wave_Properties2.html,, Jun,4, 2012
3. http://en.wikipedia.org/wiki/Group_velocity, Jun,4,2012
4. http://en.wikipedia.org/wiki/Phase_velocity, Jun, 4,2012
5. K. Nightingale, S. McAleavey, and G. Trahey, "Shear wave generation using acoustic radiation force: In vivo and ex vivo results,"Ultrasound Med. Biol, **29**(2), 1715-1723 (2003).
6. J. McLaughlin and D. Renzi, "Using level set based inversion of arrival times to recover shear wave speed in transient elastography and supersonic imaging," Inverse Probl, **22**, 707-725 (2006).
7. M. L. Palmeri, S. A. McAleavey, G. E. Trahey, and K. R. Nightingale, "Ultrasonic tracking of acoustic radiation force-induced displacements in homogeneous media," IEEE Trans. Ultrason., Ferroelectr., Freq. Control, **53**(7), 1300–1313 (2006).
8. G. F. Pinton and G. E. Trahey, "Continuous delay estimation with polynomial splines," IEEE Trans. Ultrason., Ferroelectr., Freq. Control, **53**(11), 2026-2035 (2006).
9. A. P. Sarvazyan, O. V. Rudenko, S. D. Swanson, J. B. Fowlkes, and S. Y. Emelianov, "Shear wave elasticity imaging: A new ultrasonic technology of medical diagnostics," UMB, **24**(9), 1419-1435 (1998).
10. J. McLaughlin and D. Renzi, "Shear wave speed recovery in transient elastography and supersonic imaging using propagating fronts,"Inverse Probl, **22**, 681-706 (2006).

11. M. L. Palmeri, M. H. Wang, J. J. Dahl, K. D. Frinkley, and K. R. Nightingale, "Quantifying hepatic shear modulus in vivo using acoustic radiation force," Ultrasound Med. Biol, **34**(4), 546-558 (2008).

12. A. Karpiouk, S. Aglyamov, Y. Ilinskii, E. Zabolotskaya, and S. Emelianov, "Assessment of shear modulus of tissue using ultrasound radiation force acting on a spherical acoustic inhomogeneity," IEEE Trans. Ultrason., Ferroelectr., Freq. Control, **56**(11), 2380 - 2387 (2009).

13. M. Orescanin, "Complex shear modulus reconstruction using ultrasound," Thesis, University of Illinois at Urbana-Champaign,1-185 (2010).

14. W. A. Berg, D. O. Cosgrove, C. J. Doré, F. K. W. Schäfer, W. E. Svensson, R. J. Hooley, R. Ohlinger, E. B. Mendelson, C. B-Maestro, M. Locatelli, C. Tourasse, B. C. Cavanaugh, V. Juhan, A. T. Stavros, A. Tardivon, J. Gay, J. P. Henry, and C. C-Bacrie,"Shear-wave elastography improves the specificity of breast US: the be1 multinational study of 939 masses ," *Radiology*, **262**(2),435-449(2012).

15. Fink M, Tanter M: Multiwave imaging and super resolution. Phys Today 2010, 63:28-33

16. J. Bercoff, M. Tanter, and M. Fink, "Supersonic shear imaging: A new technique for soft tissue elasticity mapping," IEEE Trans. Ultrason., Ferroelectr., Freq. Control, **51**(4), 396 - 409 (2004).

17. Jonathan Bishop, PhD Greg Poole Michael Leitch, BSc Donald B. Plewes, PhD ," Magnetic resonance imaging of shear wave propagation in excised tissue" Magnetic Resonance Imaging**,** 8(6), 1257–1265,(December 1998)

18. http://www.mayoclinic.org/magnetic-resonance-elastography).(Jun,4, 2012)

19. Kevin J. Glaser, Joel P. Felmlee,2Armando Manduca, Yogesh Kannan Mariappan,and Richard L. Ehman,Stiffness-Weighted Magnetic Resonance Imaging, Magnetic Resonance in Medicine 55:59–67 (2006)
20. Shadi F. Othman, Xiaohong Joe Zhou, Huihui Xu, Thomas J. Royston, Richard L. Magin. "Error propagation model for microscopic magnetic resonance elastography shear-wave images" Magnetic Resonance Imaging 25 (2007) 94–100
21. http://www.nrc-cnrc.gc.ca/eng/projects/ibd/oct.html, (Jun,4,2012)
22. J. M. Schmitt, "OCT elastography: imaging microscopic deformation and strain of tissue," Optic.express, **3**(6), 199-211 (1998).
23. X. Liang, M. Orescanin, K. S. Toohey, M. F. Insana, and S. A. Boppart, "Acoustomotive optical coherence elastography for measuring material mechanical properties," Opt. Letters, **34**(19), 2894-2896 (2009).
24. J. F. Greenleaf, M. Fatemi, and M. Insana, "Selected methods for imaging elastic properties of biological tissues," Annu. Rev. Biomed. Eng, **5**, 57-78 (2003).
25. Yang .Victor, Endoscopic Doppler Optical Coherence Tomography, PHD thesis ,2004
26. Murtaza Ali and Renuka Parlapalli, "Signal Processing Overview of Optical Coherence Tomography Systems for Medical Imaging" Texas Instruments,June 2010
27. Darren Morofke, " 2-D kasai velocity estimation for Doppler optical coherence tomography", Thesis,Ryerson University, 2006

28. R.C. Chan, A.H. Chau,W.C. Karl, S. Nadkarni, A.S. Khalil, N. Iftimia, M. Shishkov, G.J. Tearney, M.R. Kaazempur-Mofrad, and B. E. Bouma, "OCT-based arterial elastography: robust estimation exploiting tissue biomechanics,"Opt. Express,**12**(19),4558-4572(2004).

29. S. J. Kirkpatrick, R. K. Wang, and D. D. Duncan, "OCT-based elastography for large and small

Deformations," Opt. Express,**14**(24) ,11585-11597(2006).

30. S. G. Adie, X. Liang, B. F. Kennedy, R. John, D. D. Sampson, and S. A. Boppart, " Spectroscopic optical coherence elastography," Opt. Express,**18**(25),25519-25534(2010).

31. X. Liang, S. G. Adie, R.John, and S. A. Boppart, "Dynamic spectral-domain optical coherence

elastography for tissue characterization," Opt. Express,**18**(13),14183-14190(2010).

32. B. F. Kennedy, X. Liang, S. G. Adie, D. K. Gerstmann, B. C. Quirk, S. A. Boppart, and D.D. Sampson1, " *In vivo* three-dimensional optical coherence elastography," Opt. Express,**19**(7),6623-6634(2011).

33. X. Liang and S.A. Boppart, "Biomechanical properties of in vivo human skin from dynamic optical coherence elastography" ,**57**(4), 953-959(2010).

34. B.F. Kennedy, T. R. Hillman, R. A. McLaughlin, B. C. Quirk, and D. D. Sampson, "*In vivo* dynamic optical coherence elastography using a ring actuator," Opt. Express,,**17**(24),21762-21772(2009).

35. S. H. Yun, G. J. Tearney, J. F. de Boer, and B. E. Bouma, "Motion artifacts in optical coherence tomography with frequency-domain ranging," Opt. Express,**12**(13),2977-2998(2004).

36. A. Mariampillai, B. A. Standish, N. R. Munce, C. Randall, G. Liu, J. Y. Jiang, A. E. Cable, I. A. Vitkin, and V. Yang , "Doppler optical cardiogram gated 2D color flow imaging at 1000 fps and 4D in vivo visualization of embryonic heart at 45 fps on a swept source ," Opt. Express, **15**(4), 1627-1638 (2007).

37. K. Nightingale, S. McAleavey, and G. Trahey, "Shear wave generation using acoustic radiation force: In vivo and ex vivo results,"Ultrasound Med. Biol, **29**(2), 1715-1723 (2003).